

# Searching for SUSY in all hadronic final states with the $\alpha_T$ variable

Bryn Mathias  
Imperial College London

Supervisor: Dr Alex Tapper

## Abstract

1

2

This is a thesis.

## Declaration

There are many like it.

Author

## Acknowledgements

1

2

Thanks.

# Contents

<b>1</b>	<b>Introduction</b>	<b>6</b>
<b>2</b>	<b>Theory</b>	<b>7</b>
<b>3</b>	<b>The CMS detector</b>	<b>8</b>
<b>4</b>	<b>Level One Calorimeter Trigger</b>	<b>9</b>
4.1	Leve-1 Trigger Jet Algorithm . . . . .	10
4.2	Level-1 Trigger Performance . . . . .	13
4.3	Level-1 Trigger Pile-up Mitigation . . . . .	20
4.3.1	Effect on trigger rates . . . . .	21
4.3.2	Low Pile Up . . . . .	21
4.3.3	High Pile Up . . . . .	22
4.3.4	Effect on trigger efficiency . . . . .	23
4.3.5	Summary . . . . .	26
<b>5</b>	<b>Offline Object Deffinitions</b>	<b>27</b>
<b>6</b>	<b>The <math>\alpha_T</math> analysis</b>	<b>28</b>
<b>7</b>	<b>Conclusion</b>	<b>29</b>
	<b>Bibliography</b>	<b>31</b>

# Chapter 1

## Introduction

**The accelerator and detectors** The Large Hadron Collider (LHC) [3] is a proton-proton collider which is situated in the Large Electron Positron (LEP) tunnel approximately 100 m under the franco-swiss border. Design center of mass energy is 14 TeV with an instantaneous luminosity of  $1 \times 10^{34} \text{cm}^{-2} \text{s}^{-1}$ . However during 2011 the center of mass energy was 7 TeV and the maximum luminosity was  $5 \times 10^{33} \text{cm}^{-2} \text{s}^{-1}$ . To achieve this high energy and high beam current the LHC uses superconducting niobium-titanium magnets, cooled to a temperature of 1.8 Kelvin, that produce a maximum field strength of 8.36 Tesla.

**TODO: we might well need some more stuff about the LHC its self in here!**

Situated around the LHC ring are four detectors, two general detectors ATLAS [1] and CMS (see Chapter 3 for a detailed discussion of the CMS detector) [5][8] which are designed to measure the standard model to high precision and search for new physics. The LHC beauty experiment [7] is designed to study at previously unattainable precision the decays of heavy quark flavors, both to measure the standard model couplings and to search for beyond the standard model (BSM) physical processes. Finally the ALICE [2] experiment is designed to run when the LHC is running in it's secondary mode where rather than proton bunches, lead ions are collided, in an effort to study the quark-gluon plasma.

**New physics** Whilst the theory of the standard model and of new physics models will be discussed in chapter 2 it is prudent to discuss the observable features of these models with regard to design requirements for the general purpose detectors.

## Chapter 2

### <sub>1</sub> Theory

## Chapter 3

### <sub>1</sub> The CMS detector



# Chapter 4

## Level One Calorimeter Trigger

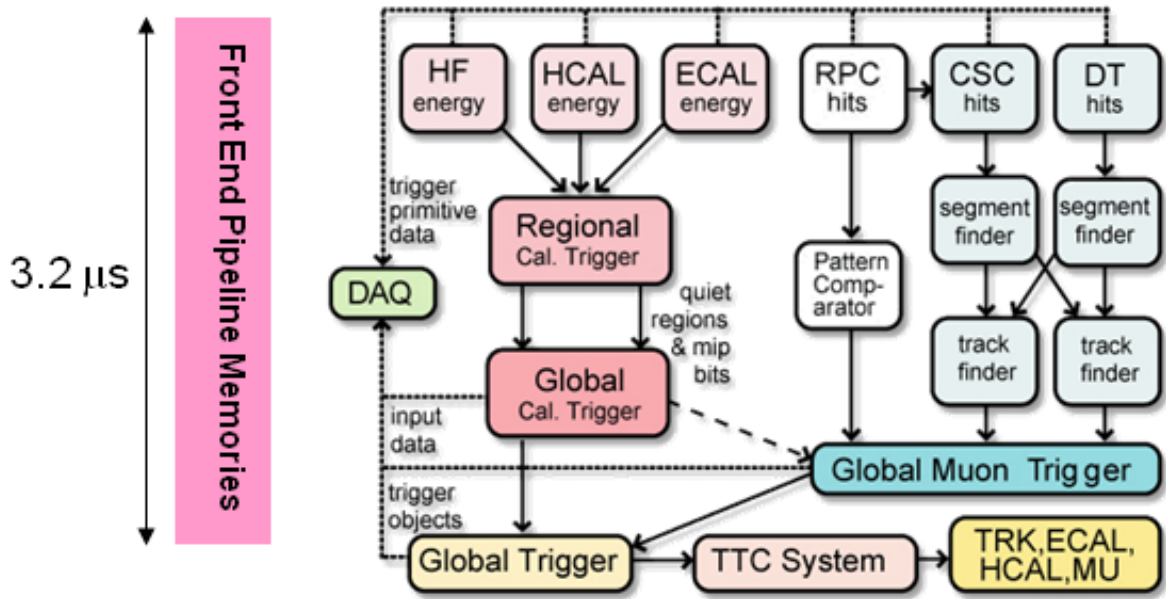


Figure 4.1: The CMS Level-1 Trigger system

The CMS Level-1 trigger system[4] is a pipelined dead-timeless system based on custom-built electronics. The Level-1 trigger is a combination of several sub systems, which are interconnected as depicted in Figure 4.1.

Coarse grain information from the electro-magnetic, hadronic and forward calorimeters is processed by the Regional Calorimeter Trigger (RCT), this is then passed to the Global Calorimeter Trigger (GCT) where the coarse grain information is clustered into physics objects, these objects are then passed to the Global Trigger where the Level-1 accept decision is made. Due to the limited size of the pipe line this Level-1 accept must be issued within  $4.0 \mu\text{s}$ .

The objects passed from the GCT to the GT include electro-magnetic objects, both electrons and photons as due to the lack of tracking information at the Level-1 trigger these objects are indistinguishable, jets and energy sums.

The RCT generates up to 72 isolated and non-isolated electro-magnetic objects, these are sorted by rank, which is equivalent to transverse energy  $E_T$ . The four highest ranked electro-magnetic objects are then passed via the GCT to the GT at an equivalent data rate of 29 Gbs<sup>-1</sup> per type.

Hadronic objects under go two clustering steps. First the transverse energy sums of the ECAL and corresponding HCAL towers are calculated, the towers are then summed in to 4×4 trigger regions, these are passed to the GCT at a data rate of 172.8 Gbs<sup>-1</sup>. These trigger regions are clustered in to jet candidates by the GCT and ranked. The jets are then sub-divided in the categories depending on their pseudo-rapidity and the result of  $\tau$  identification.

Energy sums come in two forms, the total transverse energy  $E_T$  which is the scalar sum of all transverse energies and the total jet transverse energy  $H_T$  which is calculated as the scalar sum of all jets above some programable threshold.

The missing energy equivalents of these  $E_T^{\text{miss}}$  and  $H_T^{\text{miss}}$  are formed from the negative vector sum of the objects considered for the transverse sums.

## 4.1 Leve-1 Trigger Jet Algorithm

**FIXME:** This is taken pretty much straight from [6] might want to steal less??

The CMS detector can be un-rolled in the  $\phi$  direction to form a rectangular grid of the 396 calorimeter regions, connected along the  $\phi$  edge. The rectangle 18  $\phi$  divisions (from  $-180^\circ < \phi \leq 180^\circ$ ) by 22  $\eta$  divisions ( from  $-5 < \eta < 5$ ). Each  $\phi$  division corresponds to  $20^\circ$ . The  $\eta$  divisions correspond to  $\Delta\eta = 0.5$  in the forward calorimeters and to  $\Delta\eta \approx 0.348$  in the barrel. A pictorial representation of this can be seen in figure 4.3.

A jet candidate is created if the sum of the ECAL and HCAL energies of the central calorimeter region has an energy deposit larger than all of its neighbours, as shown in figure 4.2 The jet is centered at this region where  $p_T^{\text{central}} > p_T^{\text{surrounding}}$  and the transverse energies of the surrounding regions are summed in to the central region. The jet is then

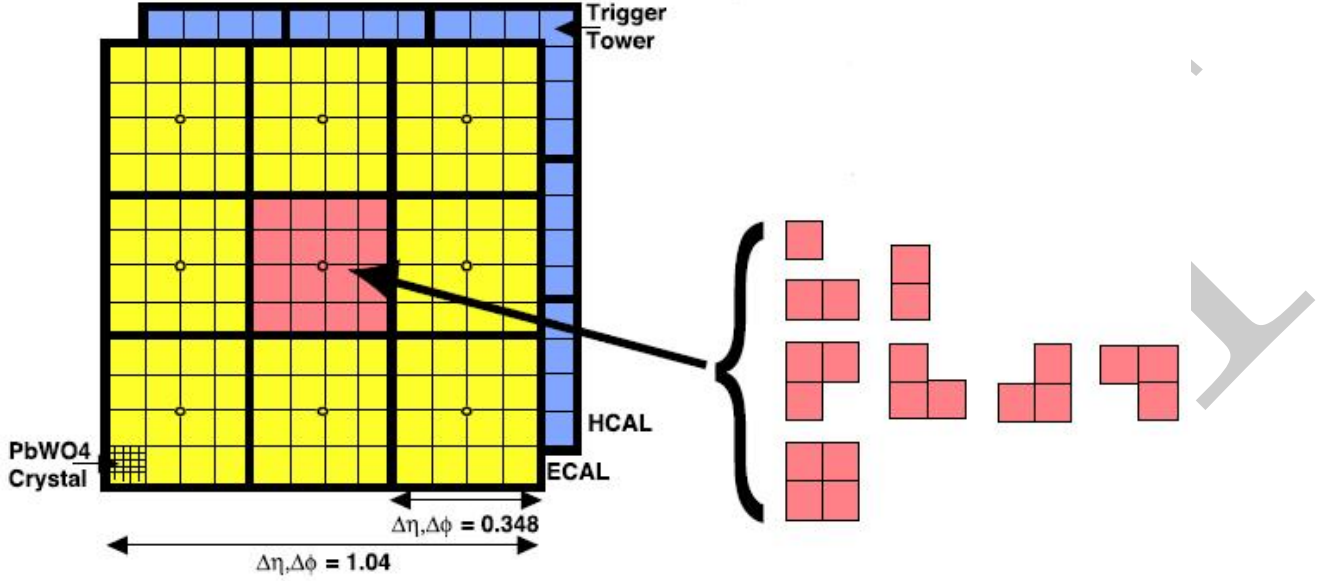


**Figure 4.2:** The  $3 \times 3$  jet-finder window at Level-1. Each cell represents a trigger tower, which is the sum of the HCAL and ECAL transverse energies. The  $\tau$ -jet veto patterns are shown to the right.

classified as a  $\tau$  jet if  $|\eta| < 3.0$  and none of the  $\tau$  veto bits are set. If any  $\tau$  vetoes are set the jet is classified as a central jet. The jet is classified as forward if  $3.0 < |\eta| < 5.0$

The  $\tau$ -vetoes are set by the RCT depending on whether or not the energy depositions in up to four contiguous trigger towers are below a programmable fraction of the regional  $E_T$  as shown in Figure 4.2.

It is possible to apply separate jet energy corrections to each of the sub categories of GCT jets. These corrections are discussed in detail in Section 4.2

In order to reduce the total data duplicated and shared between the jet finders the GCT employs a pre-clustering algorithm, which involves 18 jet finders operating simultaneously over the whole detector. These jet finders then only share information with neighboring regions when the clustered jets are found. Figure 4.3 shows the boundaries between which the jet finders operate, these map naturally on to one RCT crate per jet finder. A maximum of 3 jets can be found on each of the  $\phi$  strips acted on by the jet finders, this gives a maximum of 108 jets per event. In order to preserve continuity across the  $\eta = 0$  boundary, the two adjacent trigger regions are shared between the jet finders.

An example of the jet finding is shown in Figure 4.4. The first step is to create a  $2 \times 3$  mini cluster around any local maxima found in the  $12 \times 2$  strip. Equality statements

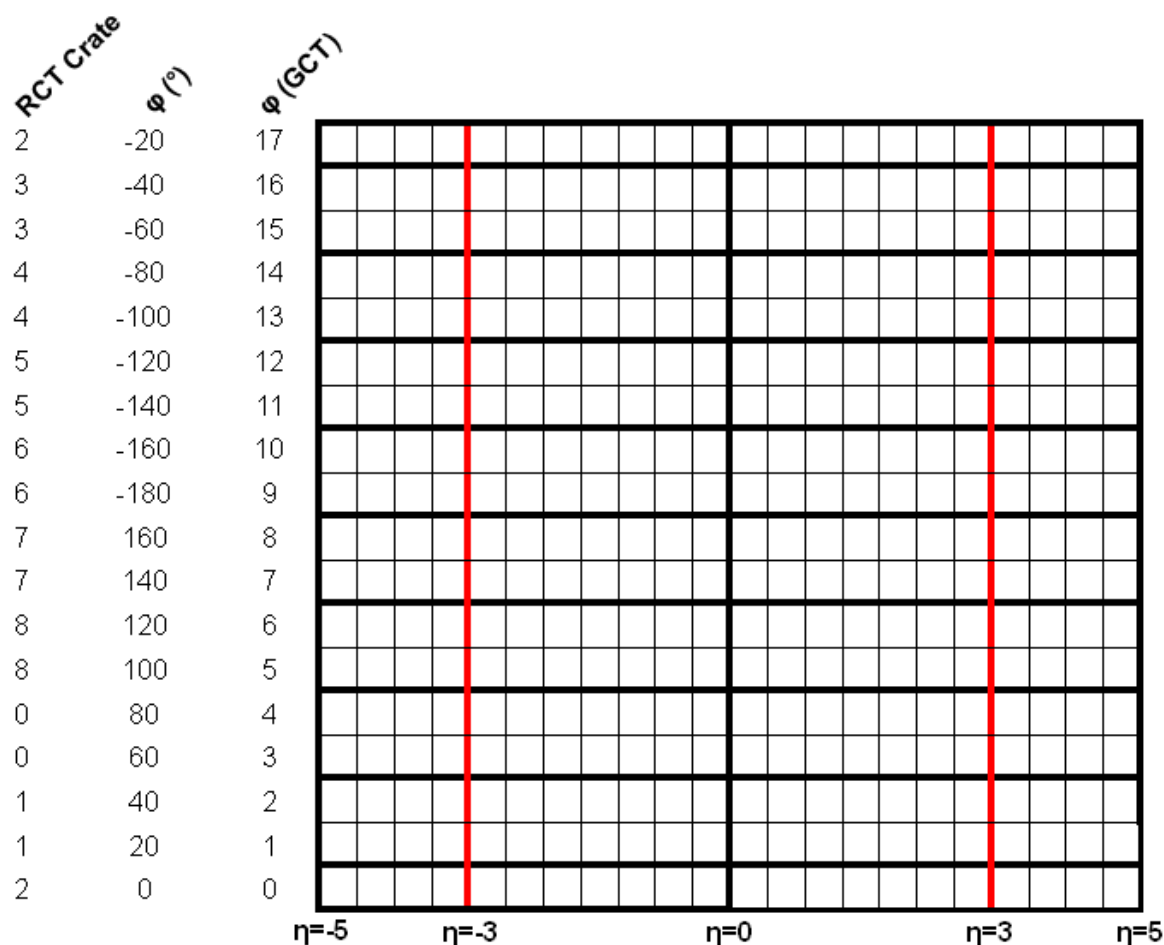


**Figure 4.3:** The calorimeter map that the  $3 \times 3$  jet-finder operates over is made up for 396 calorimeter regions, each jet finder is mapped onto an RCT crate which is composed of an  $11 \times 2$  strip of these regions. RCT crate labels are shown for negative  $\eta$  only.

are imposed so that the central cell is greater than its neighbors in some directions and greater than or equal to the neighbors other directions to enforce a gap of at least one trigger region in both  $\eta$  and  $\phi$  between the centers of the clustered jets.

In the second step the jet finder transfers the three largest mini clusters on a given  $\phi$  strip to the closest  $\phi$  strip on the neighboring jet finder. These are then compared against the existing mini clusters in that  $\phi$  strip, those that are adjacent or diagonally adjacent to a larger mini cluster are removed. The inequalities statements are then reimposed to prevent problems with clusters having the same energies. In the final stages the mini clusters have their three adjacent regions summed in to produce a  $3 \times 3$  jet cluster. Finally the four highest ranked jets are corrected and passed to the GT.

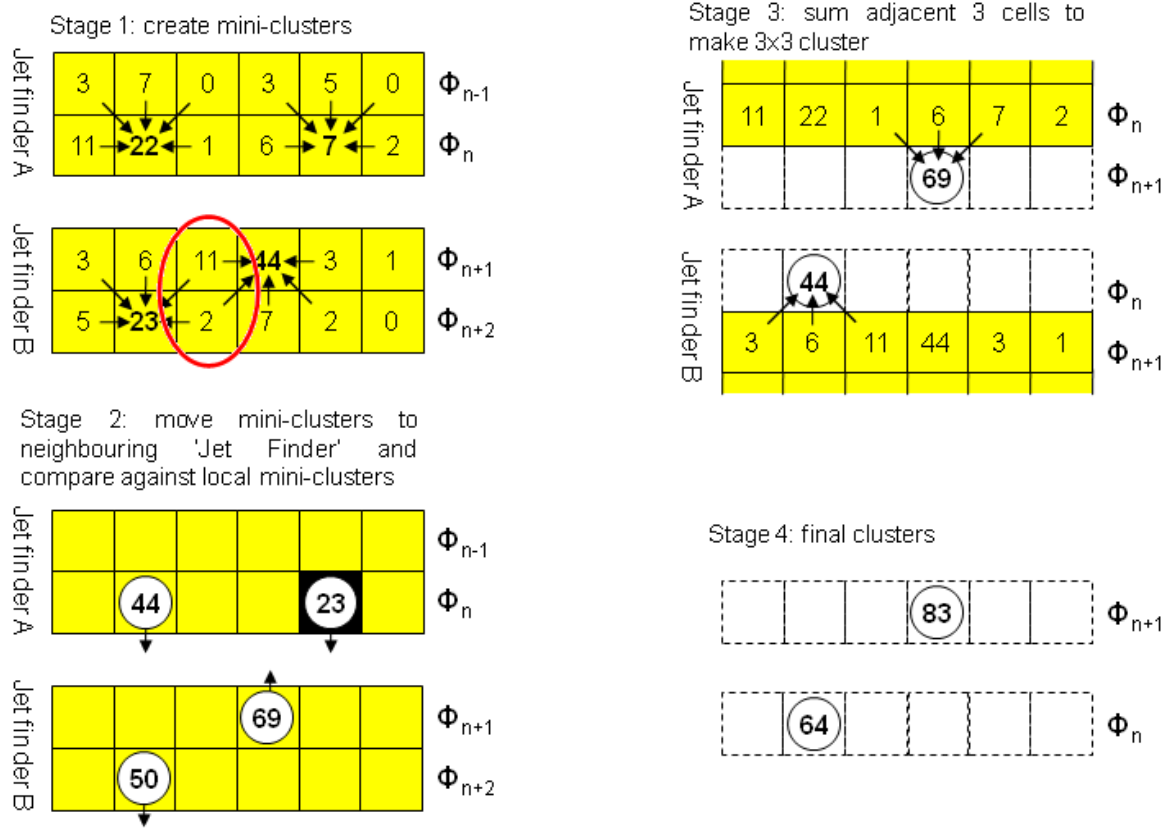


**Figure 4.4:** The Level-1 jet clustering method, six cells in  $\eta$  are shown. An example of overlapping jets is shown

## 4.2 Level-1 Trigger Performance

**FIXME:** Can i just copy the stuff out of the L1 performance note here for the corrections? I will need to re-make a bunch of the plots though :( Jobs set running as of 24th july – jobs are finally complete.

Each offline jet is matched to a Level-1 trigger jet with the smallest  $\delta R$ , for a match to be considered good  $\delta R < 0.5$  is required. The  $\delta R$  distribution is show in Figure 4.5. The energy of the leading offline matched jet is then recorded to form the denominator. To form the numerator the Level-1 jet that the offline jet is matched to is required to have an energy above some desired threshold.

To compare the performance of each of the triggers each of the turn on curves are fitted with an error function. Three example single object triggers are tested these are; L1.SingleJet16, L1.SingleJet36 and L1.SingleJet52, where the number refers to the requested  $E_T$  threshold.

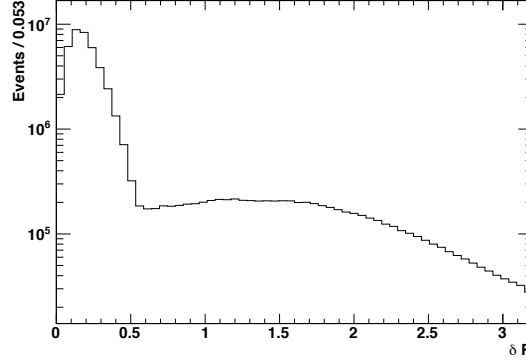


**Figure 4.5:**  $\delta R$  distribution before any selection cut, matching Level-1 jets to offline jets.

The performance is measured under two different pile up conditions, the first is where the mean number of interactions per bunch crossing ( $\langle PU \rangle$ ) is less than 16. The events studied are taken with a single  $\mu$  HLT trigger namely HLT\_IsoMu24 which requires there to be at least one muon with  $p_T \geq 24$  GeV passing loose isolation, this removes any biases on the turn on from pre selecting with a hadronic trigger. To test the performance of the trigger system under high pile up conditions ( $\langle PU \rangle \leq 32$ ) a dedicated high pile up fill of the LHC was performed. The high pile up fill is studied from two points of view, the first is with regard to standard anti- $k_t(0.5)$  calorimeter jets. Secondly the performance is measured against anti- $k_t(0.5)$  calorimeter jets that are corrected for pile up.

Figure 4.6 shows the performance of the three example Level-1 single jet triggers with the fit results listed in Table 4.1. Figure 4.7 shows the performance of the same three triggers during high pile up conditions when compared to pile up corrected anti- $k_t(0.5)$  calorimeter jets. This should be compared with Figure 4.8 where the anti- $k_t(0.5)$  calorimeter jets are not corrected for pile up. The fit results for these two sets of offline conditions are listed in Table 4.2 and 4.3 respectively.

Due to the small amount of data collected in the high pile up run there are an insufficient number of events with high  $E_T^{\text{miss}}$ ,  $H_T^{\text{miss}}$  and  $H_T$  to measure the high pile up performance. However the performance in low pile up conditions is presented below, it is noted that as there are no HLT paths seeded by a Level-1  $E_T$  trigger the performance is not measured.

Figure 4.9 shows the performance of four Level-1  $H_T$  triggers with thresholds of 50, 75, 100 and 150 GeV, the fit results to each of these performance curves is detailed in Table 4.4. The shift in  $\mu$  to larger values than the online Level-1 trigger threshold is due

to Level-1  $H_T$  being formed from the internal GCT jets before they have their energy corrected. The offline quantity is constructed using corrected anti- $k_t(0.5)$  calorimeter jets.

**FIXME:** there will be an explanation of L1FastJet corrections somewhere, point this section to it

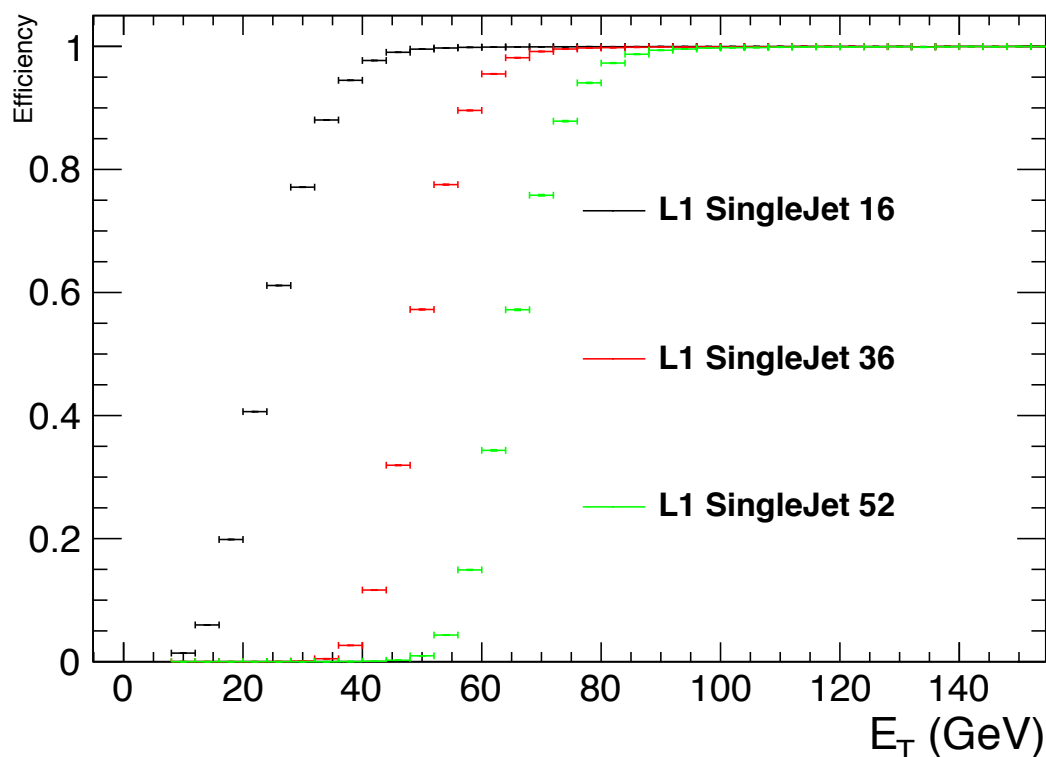


**Figure 4.6:** Turn on curves for three Level-1 single jet triggers, in terms of offline corrected anti- $k_t(0.5)$  calorimeter jet  $E_T$ .

6

7

**FIXME:** put in the run no of the HPF in here

$$fit = \frac{\epsilon}{2} \times \left(1 + \frac{2}{\sqrt{\pi}} \int_0^x e^{-t^2} dt\right) / \sqrt{2}\sigma. \text{ where } t = \epsilon - \mu \quad (4.1)$$

**FIXME: is this even right?** where  $\sigma$  describes the resolution,  $\epsilon$  gives the maximum efficiency and  $\mu$  refers to the point at which the efficiency is 50%. Throughout  $\epsilon = 1.0$  is assumed.

1

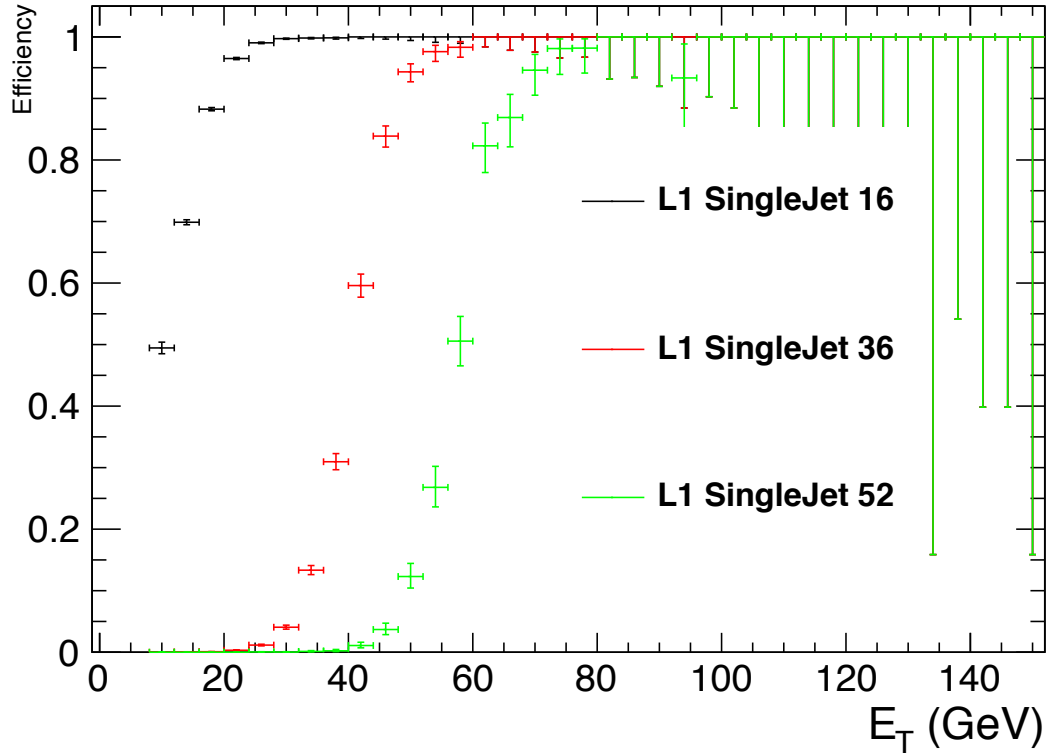


**Figure 4.7:** Turn on curves for the three Level-1 single jet triggers in terms of offline corrected anti- $k_t(0.5)$  calorimeter jet  $E_T$  in high pile up conditions.

Trigger	$\sigma$	$\mu$
L1_SingleJet16	7.48	24.27
L1_SingleJet36	6.08	49.25
L1_SingleJet52	6.75	65.11

**Table 4.1:** Results of an error function fit to the turn on curves for Level-1 single jet triggers in run 2011B. Preselected on an Isolated Muon trigger.

Trigger	$\sigma$	$\mu$
L1_SingleJet16	6.37	10.48
L1_SingleJet36	6.35	40.73
L1_SingleJet52	6.65	57.48

**Table 4.2:** Results of an error function fit to the turn on curves for Level-1 single jet triggers in the run 2011B high pile up fill Where offline hadronic objects are corrected for pile up using the FastJet calculation. Preselected on a zero bias trigger.



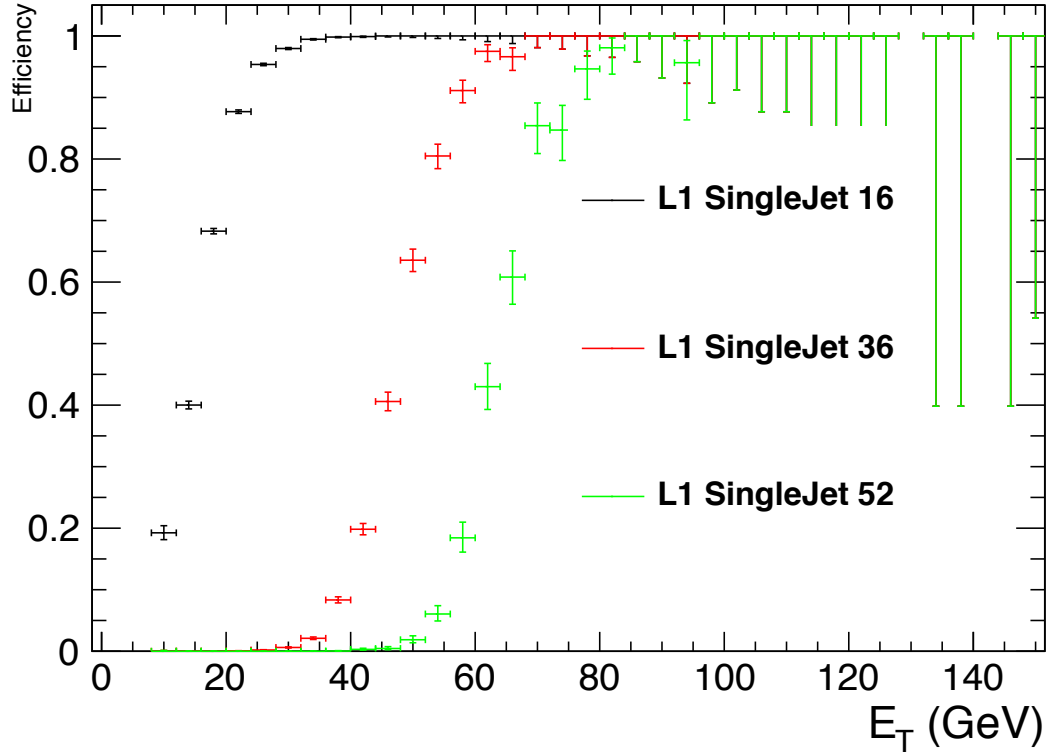


**Figure 4.8:** Turn on curves for the three Level-1 single jet triggers in terms of offline anti- $k_t(0.5)$  calorimeter jets where the energies are corrected for energy from the pile up interactions using the FastJet correction method.

Trigger	$\sigma$	$\mu$
L1_SingleJet16	6.07	15.20
L1_SingleJet36	7.05	47.77
L1_SingleJet52	6.74	63.68

**Table 4.3:** Results of an error function fit to the turn on curves for Level-1 single jet triggers in the run 2011B high pile up fill. Preselected on a zero bias trigger.

Trigger	$\sigma$	$\mu$
L1_HTT50	24.73	105.13
L1_HTT75	28.12	148.91
L1_HTT100	31.20	189.04
L1_HTT150	37.46	265.21

**Table 4.4:** Results of an error function fit to the turn on curves for Level-1 hadronic energy sum ( $H_T$ ) triggers in run 2011B. Preselected on an Isolated Muon trigger.

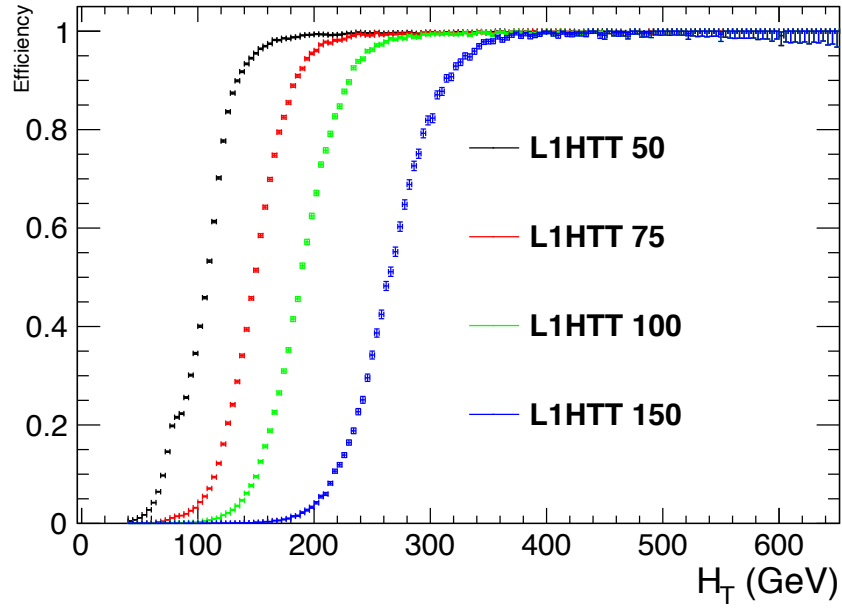


**Figure 4.9:** Turn on curves for the Level-1  $H_T$  triggers. The fit results are listed in Table 4.4

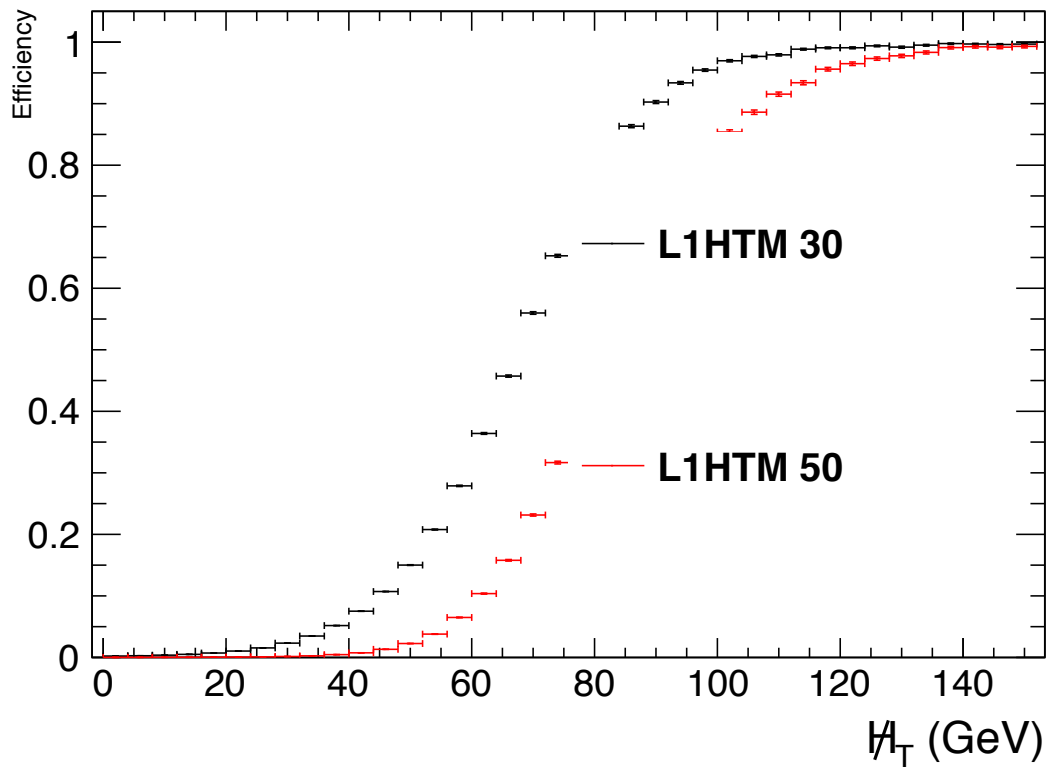


**Figure 4.10:** Performance of the Level-1  $H_T^{\text{miss}}$  triggers, preselecting on HLT\_IsoMu24. The fit results are listed in Table 4.5.

Trigger	$\sigma$	$\mu$
L1_HTM30	20.45	70.02
L1_HTM50	17.44	83.54

**Table 4.5:** Results of an error function fit to the turn on curves for Level-1 hadronic energy sum ( $H_T^{\text{miss}}$ ) triggers in run 2011B. Preselected on an Isolated Muon trigger.

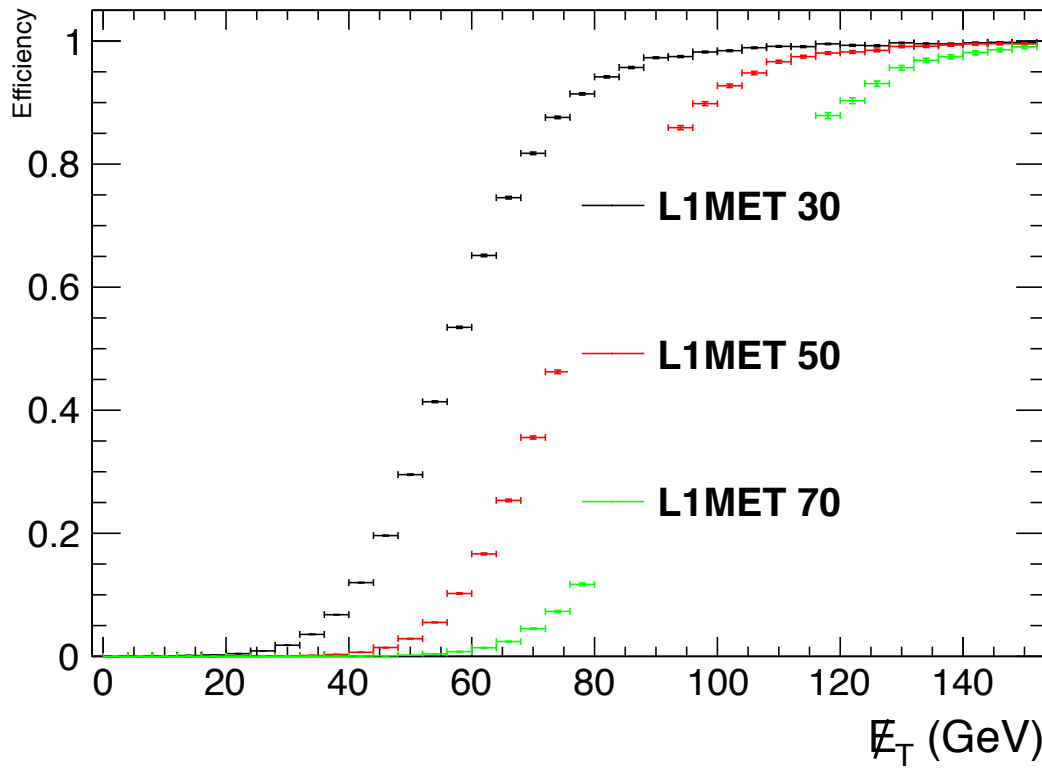


**Figure 4.11:** Performance of the Level-1  $E_T^{\text{miss}}$  triggers, preselecting on HLT\_IsoMu24. The fit results are listed in Table 4.6.

Trigger	$\sigma$	$\mu$
L1_MET30	13.53	57.65
L1_MET50	14.09	76.02
L1_MET70	16.51	97.37

**Table 4.6:** Results of an error function fit to the turn on curves for Level-1 hadronic energy sum ( $E_T^{\text{miss}}$ ) triggers in run 2011B. Preselected on an Isolated Muon trigger.

### 4.3 Level-1 Trigger Pile-up Mitigation

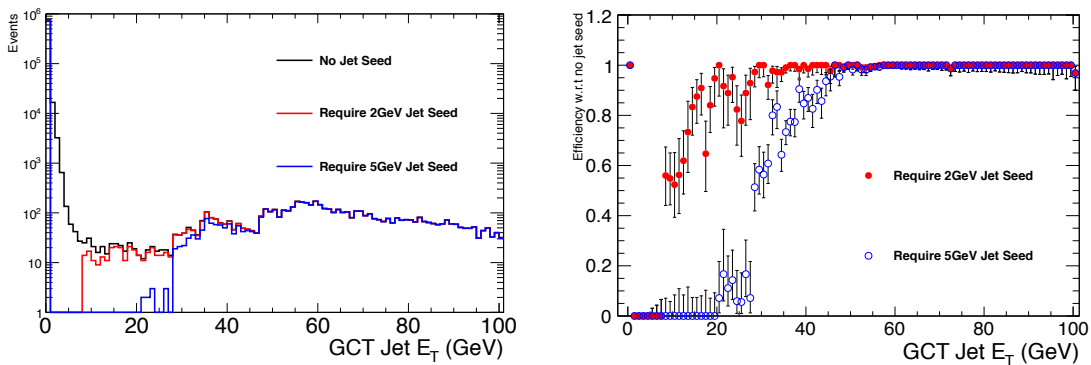
Due to the lack of a requirement of a jet seed threshold, soft non-collimated jets, such as those expected in a high pile up environment are found. Trigger decisions are then made using these pile up jets.

This is less of a problem for the single jet triggers which have a high  $P_T$  threshold. However the  $H_T$  triggers, where  $H_T = \sum_{jets} E_T^{jet}$  and the requirement of  $E_T^{jet} \geq 10$  GeV is made, see a large increase in rate due to pile-up, this is due to the low energy threshold required for a jet to be added to the  $H_T$  sum.

To counteract the effect of pile up on trigger rate we study the effects of requiring a jet seed threshold on the rate and efficiency of the individual jet and  $H_T$  triggers.

Figure 4.2 depicts  $3 \times 3$  trigger regions, each of which are built from  $4 \times 4$  trigger towers. In this case the central region is the jet seed. The proposed change would require there to be a threshold energy in the seed region.

The study of using jet seed thresholds of 2 and 5 GeV is presented. The maximum energy of effected jets is 18 GeV when requiring a seed of 2 GeV and 45 GeV when requiring a seed of 5 GeV for jets made from  $3 \times 3$  trigger regions. The jet clustering is performed before the Level-1 jets are corrected according to their  $E_T$  and  $\eta$ , hence the effects are manifested in trigger decisions for Level-1 jets above 18 or 45 GeV.



(a) GCT internal uncorrected jet  $E_T$  distributions for the same events with a 0, 2 or 5 GeV seed requirement. (b) Efficiency of applying a requirement of 2 or 5 GeV with respect to no requirement.

**Figure 4.12:** Effect of requiring a jet seed threshold on GCT internal jets.

Figure 4.12 shows how the different threshold requirements effect the rank of the internal GCT jets. The effect is to remove all jets below 2(5) GeV and to cut out jets

**Table 4.7:** Summary of rate reduction during low pile up conditions.

Trigger	% of rate taken with 2 GeV requirement	% of rate taken with 5 GeV requirement
L1_HTT100	$98.6 \pm 11.6\%$	$97.9 \pm 11.6\%$
L1_QuadJet38	$100.0 \pm 0.0\%$	$85.3 + 6.2 - 8.7\%$
L1_Jet50	$100.0 + 0.0 - 12.3\%$	$85.7 + 9.1 - 15.8\%$

from the low end of the distribution. From Figure 4.12(b) it is possible to see the point beyond which the requirement of a jet seed has no effect. For a cut of 2 GeV jets above an uncorrected  $E_T$  of  $\approx 35$  GeV are not effected, for a seed threshold of 5 GeV jets above an uncorrected  $E_T$  55 GeV are not effected.

### 4.3.1 Effect on trigger rates

The effects of applying a seed threshold are quantified in terms of the level of rate reduction in the Level-1 hadronic triggers. Three triggers are studied, they are:

- L1\_SingleJet50 - Level one trigger requiring at least one jet with a corrected  $E_T \geq 50$  GeV.
- L1\_HTT100 - Level one trigger requiring  $H_T \geq 100$  GeV.
- L1\_QuadJet38 - Level one trigger requiring at least four jets in the event with  $E_T \geq 38$  GeV.

### 4.3.2 Low Pile Up

A small effect on trigger rates in the low pile up scenario is expected due to the majority of energy deposited in the calorimeters coming from hard scattering.

Table 4.7 shows the rate reduction of requiring a 2 or 5 GeV seed threshold with respect to requiring no seed threshold.

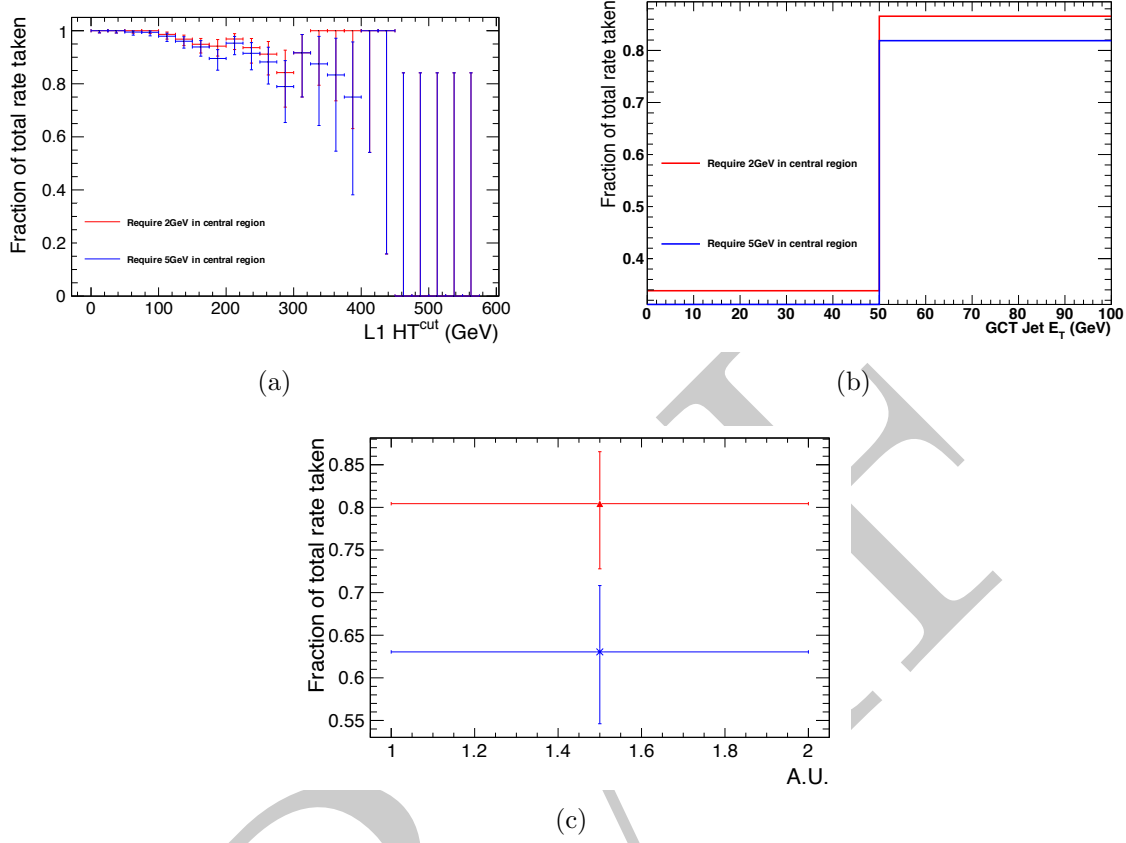


**Figure 4.13:** Rate reductions for various Level-1 algorithms when applying a 2,5 GeV seed tower requirement, in low pile up conditions. Figure (a) shows the rate reduction for  $H_T$  triggers at low pile up in cut steps of 25 GeV. Figure (b) shows the rate reduction for jets with in  $|\eta| < 3$ . and  $p_T > 50$  GeV. Figure (c) shows the rate reduction for a quad jet trigger, with jet  $|\eta| < 3$ . and  $p_T > 38$  GeV.

### 4.3.3 High Pile Up

Pile up is expected to add a small quantity of energy to the entire calorimeter system, this energy comes in the form of soft non-collimated jets. These objects are then not reconstructed if the topological cut of applying a seed threshold is required.

Table 4.8 shows the rate reduction of requiring a 2 or 5 GeV seed threshold with respect to requiring no seed threshold in high pile up conditions.

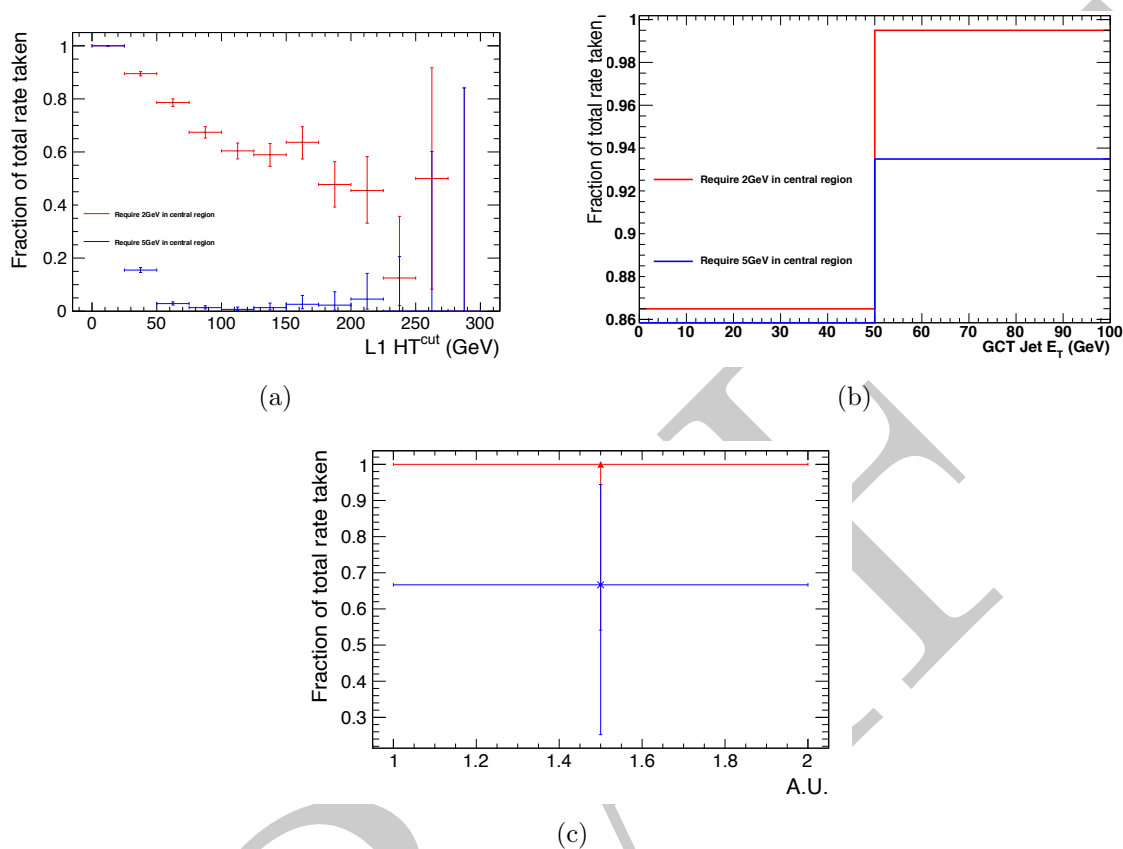


**Figure 4.14:** Rate reductions for various Level-1 algorithms when applying a 2,5 GeV seed tower requirement, in high pile up conditions. Figure (a) shows the rate reduction for  $H_T$  triggers at high pile up, in cut steps of 25 GeV. Figure (b) shows the rate reduction for jets with in  $|\eta| < 3$ . and  $p_T > 50$  GeV. Figure (c) shows the rate reduction for a quad jet trigger, with jet  $|\eta| < 3$ . and  $p_T > 38$  GeV

**Table 4.8:** Summary of rate reduction during high pile up conditions.

Trigger	% of rate taken with 2 GeV requirement	% of rate taken with 5 GeV requirement
L1_HTT100	$60.4 \pm 5.7\%$	$0.67 + / - 0.67\%$
L1_QuadJet38	$71.4 + 18.2 - 25.9\%$	$57.1 + 22.3 - 24.8\%$
L1_Jet50	$100.0 + 0.0 - 7.7\%$	$73.9 + 9.8 - 12.3\%$

## 4.3.4 Effect on trigger efficiency

Section 4.3.1 shows that requiring a jet seed threshold substantially reduces the trigger acceptance rate at in high pile up conditions.

However the aim of requiring a jet seed is to reduce rate, but not at the cost of physics. In this section we look at the effects of requiring a seed threshold, whilst requiring some loose, generic offline selection on the hadronic objects.

The change in efficiency is measured under low pile up conditions where the least extra energy added to the event. This gives a worse case estimate of the effect of requiring a jet seed on the offline efficiency.

Each offline reconstructed calorimeter jet must adhere to the following quality criteria:

- Pass loose calorimeter ID
- $p_T \geq 30$  GeV.
- $|\eta| \leq 3.0$ .
- Matched to a Level-1 jet with  $\Delta R \leq 0.5$ .

Where loose calorimeter ID is defined as; Electro-Magnetic fraction  $> 0.01$ , fraction of energy in the Hybrid Photo Diodes  $< 0.98$  and the number of n90hits  $> 1$ .

**Efficiency of  $H_T$  Triggers** Figure 4.15(a) shows the acceptance reduction after applying the two jet seed thresholds. The distribution is the cumulative number of events passing a cut of  $L1HT^{cut}$  in bins of 25 GeV. Due to  $H_T$  being the scalar sum of the jet  $p_T$ 's in the event the value of Level-1  $H_T$  is reduced as jets are removed from the calculation. To preserve efficiency the Level-1 trigger threshold will have to be reduced. Comparing figures 4.13(a) and 4.15(a), if the trigger threshold is reduced to 75 GeV an efficiency of  $\geq 95\%$  can be maintained whilst reducing the trigger rate by  $\approx 2\%$  when requiring a 2 GeV seed threshold and reduced by  $\approx 3\%$  when requiring a 5 GeV seed threshold. When comparing to the high pile up rate reduction in figure 4.14(a) it is shown that the trigger rate can be reduced by  $\approx 20\%$  when requiring a 2 GeV seed threshold and reduced by  $\geq 99\%$  when requiring a 5 GeV seed threshold.

**Efficiency of Jet Triggers** Figure 4.15(b) shows the change in acceptance of jets in low pile up conditions when the two seed thresholds are required. The effect is on the order of a few percent for each of the thresholds. Requiring a 2 GeV seed reduces the efficiency for jets above 50 GeV by  $\approx 2.5\%$ , whilst requiring a 5 GeV seed reduces the efficiency of the same jets by  $\approx 4\%$ .



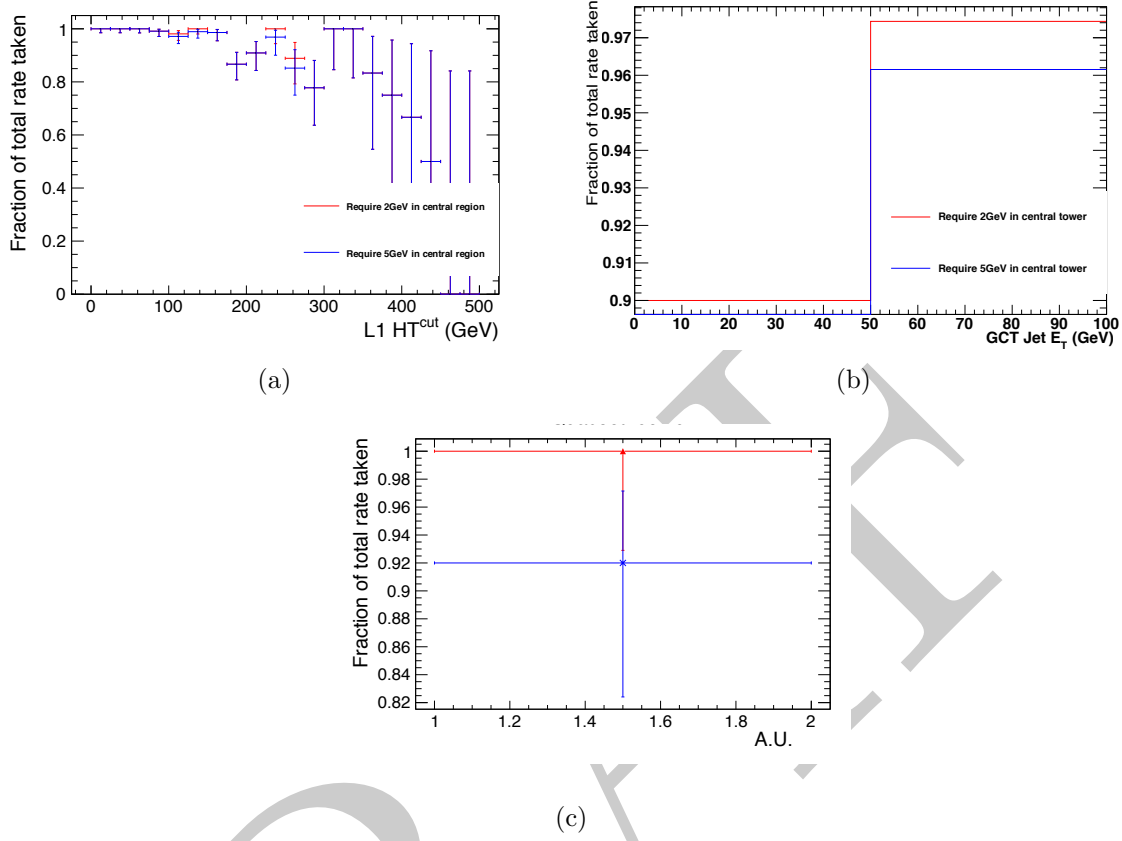


**Figure 4.15:** Efficiency reductions for various Level-1 algorithms when applying a 2 or 5 GeV seed tower requirement, in low pile up conditions. Figure (a) shows the efficiency reduction for  $H_T$  triggers at low pile up in cut steps of 25 GeV. Figure (b) shows the efficiency reduction for jets with  $|\eta| < 3$  and  $p_T > 50$  GeV. Figure (c) shows the efficiency reduction for a quad jet trigger, with jet  $|\eta| < 3$  and  $p_T > 38$  GeV.

**Efficiency of MultiJet Triggers** Figure 4.15(c) shows that the effect of requiring a seed threshold of 2 GeV has no effect on the efficiency of the quad jet 38 GeV trigger and requiring a seed threshold of 5 GeV reduces the efficiency of the quad jet 38 trigger by 8%. The change in rate is dramatic in high pile up conditions where for a 2 GeV seed threshold the rate is reduced by  $\approx 30\%$  and by  $\approx 40\%$  when requiring a 5 GeV seed. However it is to be noted that the sample where this measurement has been made is of limited size, inferring a reasonably large statistical uncertainty.

### 4.3.5 Summary

The effects of requiring a jet seed have been studied using the Level-1 trigger emulator on high and low pile-up samples. The studies show that requiring a jet seed of 5 GeV greatly reduces the rate of the  $H_T$  and Multi Jet triggers in high pile up conditions, whilst not adversely affecting the data taking efficiency of these triggers.

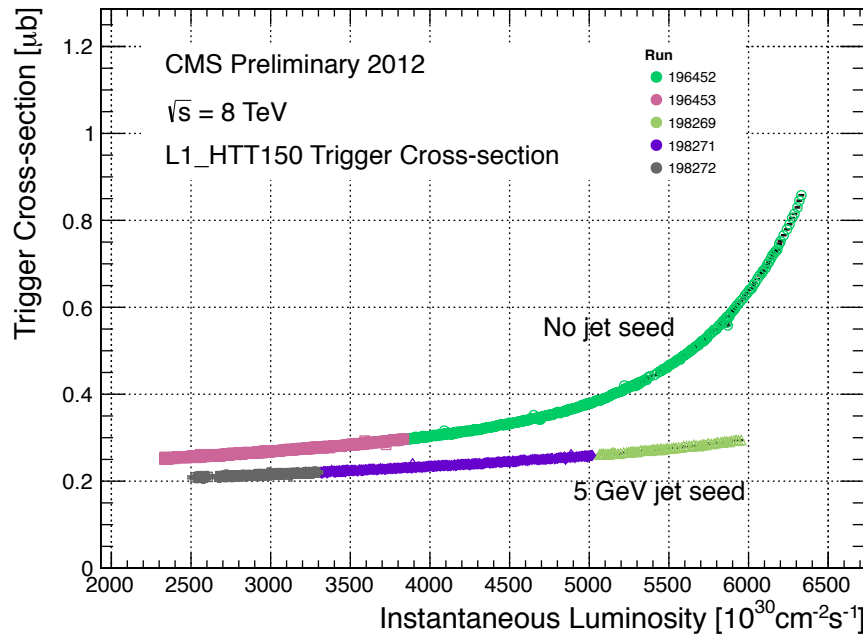


**Figure 4.16:** Trigger cross section as a function of number of pile up interactions. Showing that applying a 5 GeV jet seed threshold dramatically reduces the quadratic dependence of cross section on the number of pile up interactions

The cross section of L1\_HTT150 has been measured with and without the addition of a jet seed threshold of 5 GeV as shown in Figure 4.16. Ideally the trigger cross section would be independent of the instantaneous luminosity and pile up, Figure 4.16 shows that the addition of a 5 GeV seed threshold reduces the dependence on instantaneous luminosity of the trigger cross section.

## Chapter 5

### <sub>1</sub> Offline Object Definitions

## Chapter 6

### <sub>1</sub> The $\alpha_T$ analysis

## Chapter 7

### <sub>1</sub> Conclusion

1

DRAFT

## Bibliography

- [1] T Åkesson. The ATLAS experiment at the CERN Large Hadron Collider - CERN Document Server. *Particles*, 1999.
- [2] B Alessandro, F Antinori, J Belikov, and C Blume. ALICE: Physics performance report, volume II. *Journal of Physics G: Nuclear and Particle Physics*, January 2006.
- [3] Michael Benedikt, Paul Collier, V Mertens, John Poole, and Karlheinz Schindl. *LHC Design Report*. CERN, Geneva, 2004.
- [4] CMS Collaboration. The Trigger and Data Acquisition Project Technical Design Report, Volume 1, The Level-1 Trigger. *CERN/LHCC 2000-038, CMS TDR 6.1*, 2000.
- [5] M Friedl, N Frischauf, T Bauer, T Bergauer, W Waltenberger, A R Knapitsch, C Imler, I Kratschmer, W Treberer-treberspurg, B Rahbaran, V Innocente, T Camporesi, S Gowdy, L Malgeri, A Marchioro, L Moneta, W Weingarten, M Giunta, M Rovere, A Bonato, A C Spataru, S Zhang, A Perieanu, N Heracleous, H K V Reithler, B Philipps, M K Merschmeyer, C A Heidemann, H Geenen, Y Kuessel, E Kuznetsova, J Olzem, A Bethani, L Calligaris, R Walsh bastos rangel, T M M Dorland, G Quast, A H Dierlamm, I Katkov, R M Ulrich, F M H Stober, C Barth, X Mol, A Kornmayer, F Matorras, A Calderon tazon, A Lopez garcia, J A Brochero cifuentes, M J Bercher, M Haguenauer, Y Sirois, C M Mironov, P Depasse, L Sgandurra, G P Heath, Z Meng, D A Hartley, N I Geddes, S Quinton, I R Tomalin, K Harder, V B Francis, Z Zhang, T Geralis, D Loukas, I Topsis giotis, G Bencze, S T Hernath, I Szeberenyi, S Banerjee, S Singh, A Colaleo, G P Maggi, M Maggi, F Loddo, R Campanini, I D'antone, C Grandi, L Guiducci, M Gulmini, S Fantinel, P Meridiani, K K Joo, S Song, J Rhee, E Won, M Jo, H Kim, D H Kim, G N Kim, J E Kim, T Son, W M Dominik, K Bunkowski, J C Rasteiro da silva, J Varela, A Alves, V Sulimov, A Vorobyev, V Murzin, S Lukyanenko, G Mesyats, V Postoev, A Pashenkov, A Solovey, S Troitsky, N Lychkovskaya, G Safronov, A Fedotov, K Olimov, M Fazilov, A Umaraliev,

I Dumanoglu, N M Bakirci, C Dozen, M Zeyrek, M Yalvac, S Ozkorucuklu, K Sevim, Y Chang, W T Lin, S Bahinipati, K A Biery, E E Gottschalk, K Maeshima, T Kramer, S W L Kwan, S J Murray, L Taylor, N Mokhov, J M Marraffino, S Mrenna, V Yarba, B Banerjee, V D Elvira, D C Hare, B Holzman, F X Yumiceva del pozo, W Dagenhart, C L Dumitrescu, S C Ryu, B J Kilminster, J K Adelman-mc carthy, V E Bazterra, I Bucinskaite, P E Karchin, J R Incandela, M D'Alfonso, R Rossin, C A West, J L Gran, G Zilizi, P P Raics, A Bhardwaj, M Naimuddin, A Kumar, N Smiljkovic, C P De oliveira martins, M Petek, A Vercosa custodio, E J Tonelli manganote, M T Narjanen, P Graehling, F Blekman, J M Keaveney, S Blyweert, N van Remortel, X J Janssen, D Druzhkin, M Bansal, A Aleksandrov, M F Shopova, T R Fernandez perez tomei, C Krug, A A Shinoda, T V Rohe, P Arce, M Daniel, J J Navarrete marin, I Redondo fernandez, A Guirao elias, J Santaolalla camino, J Lottin, P Gras, F Kircher, B Levesy, A Payn, A K Nayak, V Bhatnagar, C Randieri, M Bruzzi, O Starodubtsev, A Tropiano, D Piccolo, C Sciacca, S Meola, A Saccomanno, M Esposito, P Azzi, E Conti, S Lacaprara, M Margoni, M Sgaravatto, N Pozzobon, P Torre, B Checcucci, L Fanò, S Taroni, A Lucaroni, F Romeo, G Bagliesi, M A Ciocci, A Giassi, T Boccali, S Arezzini, A Rizzi, G Broccolo, D Dattola, C Mariotti, A Ballestrero, E Camacho-Pérez, R Magaña-Villalba, J Martínez-Ortega, M Górski, G Wrochna, M J Bluj, A Zarubin, M Nozdrin, V Ladygin, A Golunov, A Sotnikov, N Evdokimov, I Lokhtin, A Ershov, N Tyurin, S Akimenko, V Talov, N Belikov, A Ryazanov, G W Hou, Y Chao, J Alwall, X Shi, D R Wood, D C Baumgartel, J Zhang, P D Luckey, K C Sumorok, G Gomez ceballos retuerto, S H Jaditz, G S Stephans, T Ma, P J Lehtonen, M H Chan, I J Moul, R A Ofierzynski, A Pozdnyakov, B L Pollack, P B Padley, A H Adair, W J Clarida, E Tiras, G Cerizza, M Pieri, V A Sharma, M W Lebourgeois, M Norman, F Golf, M J Murray, J L S Bowen, K Buterbaugh, M Sharma, J Bunn, H Newman, M Gataullin, M Spiropulu, J Veverka, S D Thomas, K J Rose, S M Panwalkar, A Calamba, Z Xie, J S Werner, A M Zuranski, A Ferapontov, E M Laird, G Kukartsev, Z Mao, S J Wimpenny, S Gleyzer, M G Weinberg, V Veeraraghavan, and J... Bochenek. CMS - The Compact Muon Solenoid. January 1996.

[6] J Marrouche and others. Commissioning the CMS Global Calorimeter Trigger. *CMS IN*, 2010/029, 2010.

[7] J Rademacker. LHCb: Status and Physics Prospects. *Arxiv preprint hep-ex*, January 2005.

[8] C Wulz. The CMS experiment at CERN. *cdsweb.cern.ch*.